Catalysis Science & Technology

PAPER

View Article Online
View Journal

Cite this: DOI: 10.1039/c4cy01442a

Mechanistic insight into the *Z–E* isomerization catalysis of azobenzenes mediated by bare and core–shell gold nanoparticles†

Sabrina Simoncelli[ac] and Pedro F. Aramendía*[ab]

Received 4th November 2014,
Accepted 5th January 2015

DOI: 10.1039/c4cy01442a

www.rsc.org/catalysis

We explored the catalytic effect of 15 nm diameter gold nanoparticles (AuNPs) upon the thermal *Z–E* isomerization reaction of azobenzene and nine 4 and 4-4′ substituted azobenzenes (ABs). The kinetics follows a first order rate in ranges of [ABs] = 5 to 50 μM and [AuNPs] = 50 pM to 1 nM. A kinetic analysis of this compartmentalized system renders the thermal *Z–E* isomerization rate constant associated with each AuNP. Enhancements of 10- to 10^6-fold were measured for this rate constant in comparison to the same free ABs in solution. Experiments with selective Au facet coverage, as well as the kinetics studied in gold–silica core–shell nanoparticles (AuNP@SiO_2) of different thicknesses, demonstrate the surface nature of the catalysis and allow one to evaluate the diffusion coefficient of azobenzene in the silica layer.

Introduction

The interaction of metallic nanoparticles (NPs) with azobenzenes has received considerable attention during the past decades in view of the changes that the photochromic transformation confers to nanoparticle properties and photocontrollable layers on metal surfaces.[1] The adsorption of switchable molecules onto NPs can modify the optical properties of the latter either by local variation of the dielectric constant of the encompassing medium, due to the changes in the electronic properties of the isomers,[2,3] or by controlling the proximity or state of aggregation of the particles upon photoisomerization.[4–6] The isomerization efficiency of photochromic probes located in the vicinity of a NP has also attracted great interest. Metallic NPs can deactivate the electronic state of organic molecules placed near their surface through energy transfer, thus modulating the switching capability of the probe. This is a function of the photochromic–NP distance.[7] In this approach, Whitesell *et al.*[8] reported a ~100-fold increase in the isomerization quantum yield of azobenzenes located at ~1.25 nm from the surface of a 2.5 nm diameter gold nanoparticle (AuNP) with respect to the ones located at ~0.54 nm. An appealing but less studied aspect of the interaction is the analysis of the isomerization kinetic rates of azobenzenes placed near metallic NPs. In 2008, Shin *et al.* investigated the kinetic rates of *E–Z* photoconversion and *Z–E* thermal isomerization of an azobenzene (AB)–alkanethiol self-assembled layer around a 2 nm diameter AuNP.[9] They reported an increase between two and three times, respectively, for the isomerization rate constants compared to that of the free dye in solution. On the other hand, the group of Tamada *et al.* obtained identical reaction kinetic rates for a 5.2 nm diameter AuNP capped with 4-hexyl-4′-(12-(dodecyldithio)dodecyloxy)azobenzene and free AB molecules.[10] Prior to the work of Yoon *et al.* in 2011, nobody had outlined a detailed picture of the interactions involved in the isomerization of azobenzenes near the surface of metallic NPs.[4] In this report, by using surface enhanced Raman spectroscopy measurements, a 15-fold acceleration in the thermal *Z–E* isomerization kinetic rate of azobenzenes linked to AuNP aggregates was attributed to the weakening of the N–N double bond of the *Z*-AB isomer near the metallic surface. Further, Scaiano *et al.* were the first ones to report the AuNP catalysis of the thermal *Z–E* isomerization of unbounded 4 and 4-4′-substituted ABs in suspensions of 'pseudo-naked' AuNPs.[11] In this case, the proposed mechanism involves the formation of an azobenzene radical cation intermediate through electron transfer from the probe to the gold surface. In this work, average rates were measured in this AuNP suspension in water. In this contribution, we have

[a] *Centro de Investigaciones en Bionanociencias "Elizabeth Jares-Erijman" (CIBION-CONICET), Godoy Cruz 2390, 1425 Buenos Aires, Argentina. E-mail: pedro.aramendia@cibion.conicet.gov.ar*

[b] *Departamento de Química Inorgánica, Analítica y Química Física, Facultad de Ciencias Exactas y Naturales, Universidad de Buenos Aires, Pabellón 2, Ciudad Universitaria, 1428 Buenos Aires, Argentina*

[c] *Instituto de Química Física de Materiales, Ambiente y Energía (INQUIMAE-CONICET), Pabellón 2, Ciudad Universitaria, 1428 Buenos Aires, Argentina*

† Electronic supplementary information (ESI) available: Gold nanoparticle characterization, kinetic traces for NO_2-DAB, DABCYL and NO_2-HAB thermal *Z–E* isomerization, pH control experiments, global kinetic rate influence on the relative ABs–AuNPs concentration, kinetic traces for the *Z–E* isomerization of AB in suspensions of different thicknesses of AuNPs@SiO_2, determination of the AuNP associated first order thermal isomerization rate constant, and derivation of the diffusion equation. See DOI: 10.1039/c4cy01442a

thus examined the kinetics of the thermal *Z–E* isomerization for a family of 4 or 4-4′ substituted azobenzenes in AuNP suspensions with the aim of answering the following questions: What is the magnitude of the catalytic effect of the AuNPs? Can we obtain the *Z–E* thermal isomerization rate of azobenzenes over the AuNPs? What is the role of the metallic surface? Is it necessary for the photochromic compound to be in direct contact with the metallic surface or does the NP influence on the catalysis extend in volume due to the high polarizability of the NP plasmonic interaction? What is the influence of the substituents in the isomerization catalysis? What is the role of the pH of the medium?

Results

Fig. 1 shows transmission electron microscopy (TEM) micrographs and histograms of the size distribution of the AuNP and the silica coated AuNP (AuNP@SiO_2) used in this work. AuNPs are highly monodisperse (with a diameter of 15 ± 1 nm, standard deviation). On the other hand, the obtained AuNPs@SiO_2 exhibit >99% effectiveness in the coating process but a thickness standard deviation in the order of 20%.

Catalyzed *Z–E* thermal isomerization by AuNPs was observed for AB (Fig. 2) and the following nine 4 or 4-4′ substituted azobenzenes: DM-AB, DC-AB, DEO-AB, MO-AB, NO_2-AB, NO_2-MOAB, NO_2-DAB, DABCYL and NO_2-HAB (Fig. 3 and S3†). Fig. 2, 3, and S3† show the temporal spectral evolution of azobenzenes in a AuNP suspension. The spectral information of the AuNP/azobenzene systems corresponds to the characteristic spectral changes of the $Z \rightarrow E$ isomerization reaction for the free dye in solution, for example, for AB, increase of the π–π* band (λ_{max} ~ 320 nm) and decrease of the n–π* band (λ_{max} ~ 450 nm) (Fig. 2-A), and they are invariant in the presence of AuNPs.[12,13]

The small scattering by the AuNP did not affect the measurements since the kinetic data were derived from differential absorption data (see Fig. 2 and 3).

Fig. 2-B and S3† as well as the insets in Fig. 3 display the time evolution of the build-up of the *E* isomer in AuNP suspensions. The kinetics follows a first order rate with very good approximation in all cases and in ranges of [ABs] = 5 to 50 μM and [AuNPs] = 50 pM to 1 nM. This points to the fact

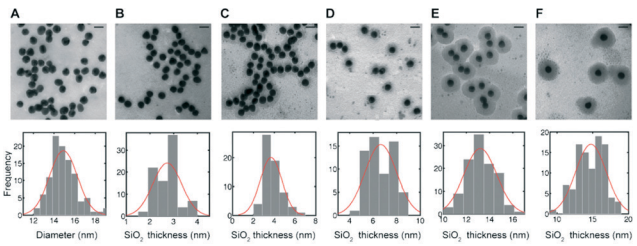

Fig. 1 TEM micrographs (upper panel) and size histograms (lower panel) of (A) AuNPs of 15 ± 1 nm diameter and AuNP@SiO_2 with increasing SiO_2 shell thicknesses of (B) 2.7 ± 0.6 nm, (C) 4 ± 1 nm, (D) 7 ± 1 nm, (E) 13 ± 1 nm and (F) 15 ± 2 nm. Scale bars: 20 nm in all cases. Histograms were constructed with sample set size $n > 50$.

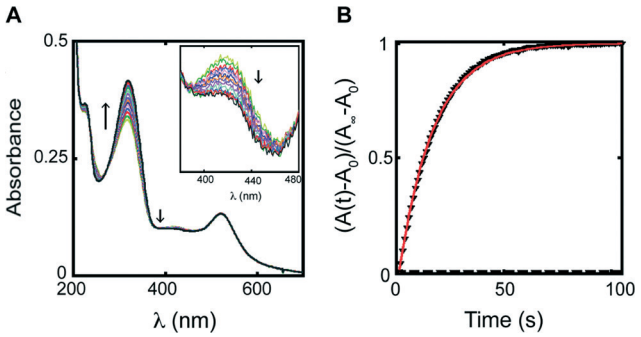

Fig. 2 (A) UV-Vis temporal evolution of a 15 μM AB aqueous solution with 300 pM AuNP suspension (diameter = 15 ± 1 nm) measured after UV flash photolysis. The inset shows the enlarged spectral region of the n–π* band. The band with a maximum at around 520 nm represents the AuNP extinction. (B) Growth of the *E* isomer concentration measured at 320 nm (black triangles). The red line is the monoexponential fit to the experimental data. The dashed black line near the abscissa axis represents the temporal evolution of the *E* isomer in the absence of AuNPs in this time interval.

that the *Z–E* isomerization is rate determining compared to other dynamic events. Specifically, the addition of 0.3 to 0.4 nM AuNPs of 15 nm diameter to 10 μM azobenzene solutions resulted in accelerated *Z–E* isomerization. The high activity of AuNP catalysis gives rise to a 10^4-fold increase in the global first order isomerization rate constant, k_{obs}, of AB and MO-AB in suspensions of AuNPs in water. On the other hand, for the systems of AuNPs and symmetrically substituted azobenzenes (DM-AB, DC-AB, and DEO-AB) in mixtures of acetonitrile (ACN) : water (5 : 1) the isomerization reaction is accelerated ~100 times with respect to the free dye in solution. For NO_2-AB and NO_2-MOAB (also in 5 : 1 ACN : water) the

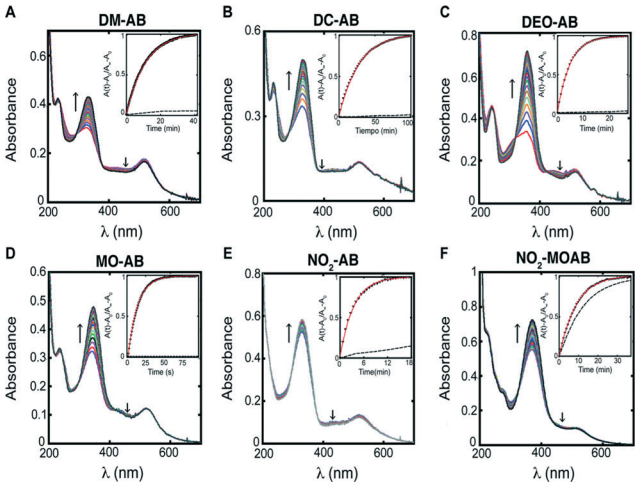

Fig. 3 UV-Vis temporal evolution of a 300 pM or 400 pM AuNP suspension (diameter = 15 ± 1 nm) and 10 μM azobenzene (A) DM-AB, (B) DC-AB, (C) DEO-AB, (D) MO-AB, (E) NO_2-AB and (F) NO_2-MOAB solutions after UV flash photolysis. The inset corresponds to the growth of the *E* isomer concentration measured at (A) 330 nm, (B) 330 nm, (C) 360 nm, (D) 345 nm, (E) 330 nm, and (F) 370 nm. The red lines represent the monoexponential fit to the experimental data. The dashed black line corresponds to the temporal evolution of the *E* isomer in the absence of AuNPs in the same time interval.

catalytic acceleration of the *Z*–*E* isomerization is much lower, with factors of 30 and 2, respectively. Regarding NO_2-DAB and DABCYL a 10^3 times increase is observed for the thermal isomerization rate, while a 50-fold increase is detected for NO_2-HAB.

The addition of AuNPs to the reaction medium provokes a decrease in the pH. Further, it is well known that acidic pH highly increases the *Z*–*E* thermal isomerization rate in azobenzenes.[14–17] Therefore, control experiments were performed for azobenzene solutions at the same pH of the AuNP suspensions but in the absence of AuNPs. The isomerization kinetics for AB, DM-AB, DC-AB, DEO-AB, MO-AB, NO_2-AB and NO_2-MOAB, in such control experiments, were identical to the ones observed for the corresponding azobenzenes in solution in the absence of acid and AuNPs (see Fig. S4†). On the other hand, for NO_2-DAB, DABCYL and NO_2-HAB the isomerization rate constants for samples with the same pH are identical, regardless of the presence or absence of AuNPs (see Fig. S5†). Thus, a potential AuNP catalytic action upon the thermal *Z*–*E* isomerization reaction for these three last mentioned azobenzenes is masked by the changes in acidity that AuNP addition causes to the solution.

Fig. 4-A and B illustrate the dependence of k_{obs} with [AuNP] and [AB] concentrations, respectively.

The trends can be interpreted considering a reaction scenery where *Z* isomers decay to the stable *E* form either in the continuous solution phase or under the influence of the dispersed AuNPs that accelerate the reaction rate. Thus, the increase of k_{obs} with AuNP concentration is related to the increase in the relative amount of *Z* molecules influenced by AuNPs. On the other hand, the increase of AB in the medium decreases the molar fraction of AB molecules associated with AuNPs, which in turn is manifested as a decreased reaction rate constant. From these experiments it stands out that the magnitude of the observed $Z \rightarrow E$ first-order kinetic rate constant only depends on the relative AB–AuNP concentration (see Fig. 5 and S7†).

The catalytic surface of a metal is heterogeneous by nature.[18] One of the main objectives in catalysis is to determine the number of catalytically different sites and the contribution of each of them in global reaction. In this regard, a common approach is to use target-blocking agents to determine the changes of reactivity.[19,20] Polyvinylpyrrolidone (PVP) selectively binds to gold and silver {100} facets.[21] On the other hand, sodium citrate binds stronger to {111} compared to {100} facets. Therefore, we decided to functionalize the citrate stabilized 15 nm AuNPs (bare AuNPs) with PVP, poisoning the catalytic activity of the {100} facets of the AuNPs. Fig. 6 shows k_{obs} as a function of the relative concentration of *Z*-AB and AuNPs for experiments with (empty circles) and without (black triangles) PVP functionalization.

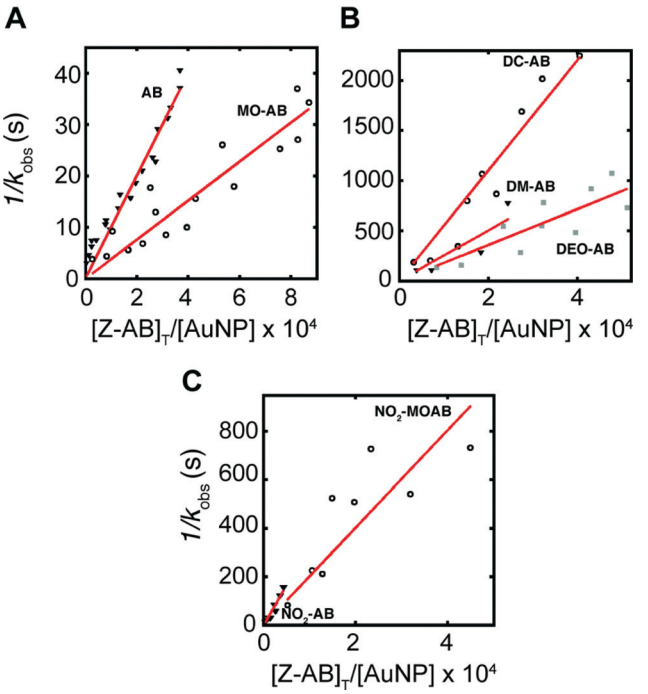

Fig. 5 Inverse of the thermal *Z*–*E* isomerization reaction rate constant as a function of the $[Z\text{-AB}]_T/[\text{AuNP}]$ for (A) aqueous and (B–C) ACN : water (5 : 1) solutions of different azobenzene/AuNP systems. The red line represents the best linear fit (see eqn (2)).

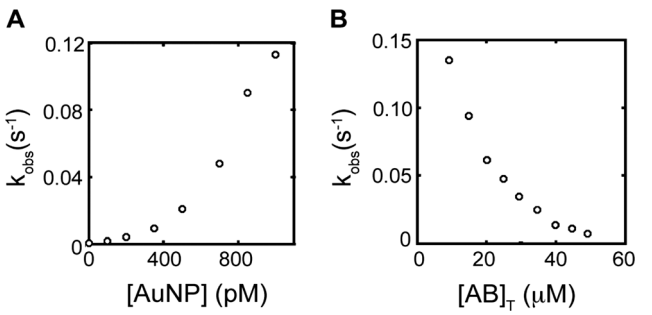

Fig. 4 Dependence of the *Z*–*E* thermal isomerization first order rate constant for an aqueous solution (A) on the AuNP concentration (50 μM AB) and (B) on the AB concentration (300 pM AuNPs). The diameter of the AuNPs is 15 ± 1 nm.

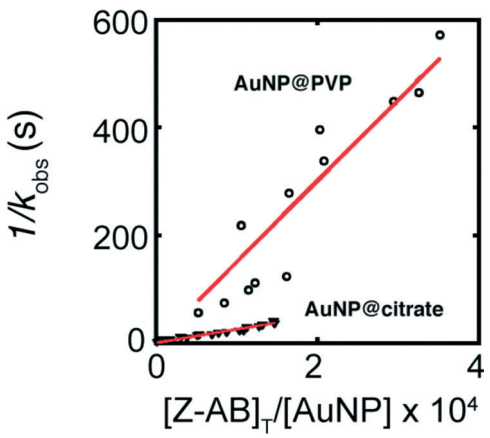

Fig. 6 Inverse of the thermal *Z*–*E* isomerization reaction rate constant as a function of the $[Z\text{-AB}]_T/[\text{AuNP}]$ for aqueous solution of azobenzenes and citrate stabilized (black triangles) or PVP-functionalized AuNPs (empty circles). The red line represents the best linear fit (see eqn (2)).

Interestingly, PVP-functionalized AuNP samples are much less efficient for the catalyzed thermal *Z*–*E* isomerization reaction than the bare-AuNPs. This can be explained as a decrease in the number of AB binding sites per AuNP in the presence of PVP to the more reactive {100} facets.

Time dependence evolution of the catalytic growth of *E*-AB by PVP-covered (blue circles) and silica-coated (green triangles and red squares) AuNPs is presented in Fig. 7.

AuNPs@SiO_2 synthesis requires transferring AuNPs from water to ethanol solutions using PVP as the coupling agent. Thus, bare AuNPs were functionalized with PVP and dispersed in ethanolic media for strict data comparison. Adsorption effects over SiO_2 were discarded in a control experiment that gave equal isomerization rate constants for free AB in solution and for AB in suspensions of silica NPs (without a Au core) (dashed line, Fig. 7). The *Z*–*E* isomerization rate constant for AB in suspensions of PVP functionalized AuNPs is ~35-fold higher than the corresponding for suspensions of AuNPs@SiO_2 with 4 ± 1 nm thickness. Further, the sigmoidal temporal dependence for the *E*-AB growth observed for core–shell NPs with a silica shell thickness of 15 ± 2 nm (red squares, Fig. 7) points to a diffusion controlled process. Specifically, immediately after NP addition, there is an initial time delay that allows *Z*-AB molecules to diffuse sufficiently close to the Au core to exhibit *Z*–*E* catalyzed reaction. The exponential increase of the absorbance of the *E* isomer is delayed as the reaction proceeds to complete conversion to this isomer.

Evaluation of the diffusion regime observed in the different silica shell thicknesses of AuNPs@SiO_2 was performed by comparing the temporal build-up of the *E* concentration

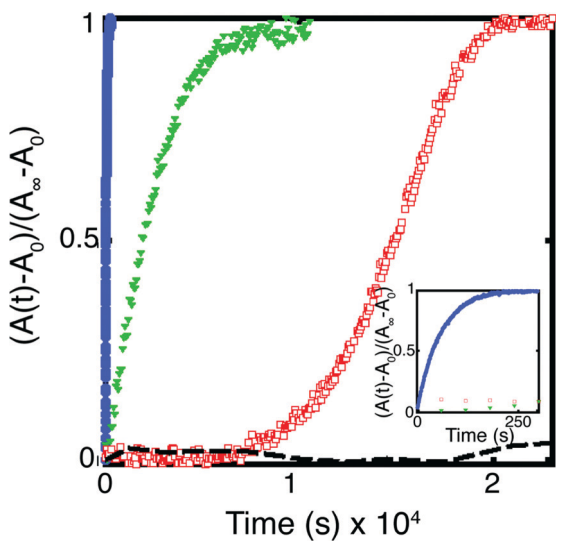

Fig. 7 Growth of the *E*-AB isomer concentration measured at 320 nm for ethanolic solutions of 8 μM AB in suspension of the following: 2 nM, 15 ± 1 nm diameter, PVP functionalized AuNPs (blue circles); 1 nM AuNPs@SiO_2 with 4 ± 1 nm (green triangles); 15 ± 2 nm (red squares) silica shell thickness; and 2 nM 71 ± 8 diameter silica nanoparticles (black dashed line) immediately after the addition of NPs and UV flash photolysis. The inset corresponds to a time range expansion for the reaction catalyzed by PVP covered gold nanoparticles.

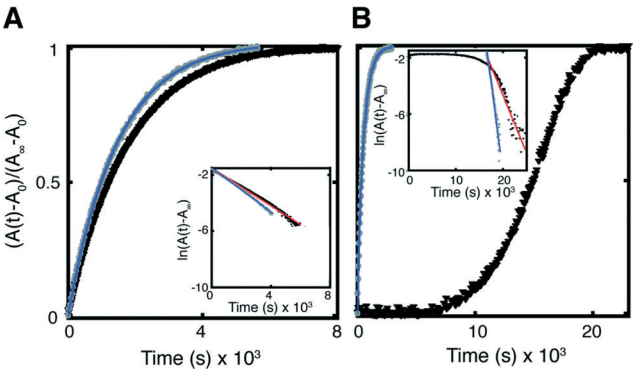

Fig. 8 Growth of the *E*-AB isomer concentration measured at 320 nm for ethanolic solutions of 8 μM AB in suspension of AuNPs@SiO_2: (A) 2.7 ± 0.6 nm ([AuNP] = 0.8 nM) and (B) 15 ± 2 nm ([AuNP] = 1.0 nM) silica shell thicknesses immediately after (black triangles) or after 12 h (grey circles) of NP addition. The blue lines are the monoexponential fits to the data. The insets correspond to the logarithmic representation of the absorbance growth. The data recorded immediately after NP addition were temporally delayed for a better comparison. The blue and red lines correspond to the best linear fits.

isomer immediately after NP addition (Fig. 8, black triangles) and after leaving the AB/AuNPs@SiO_2 solution to incubate in the dark overnight (Fig. 8, grey circles). The thinner silica shell AuNPs@SiO_2 tested, 2.7 ± 0.6 nm, displays almost the same temporal dependence for the *E* isomer growth, independent of the mixing time in the dark before photolysis (Fig. 8-A). Therefore, AB reaches a stationary diffusion regime in the silica layer during the *Z* isomer decay for this thickness. On the other hand, for NPs with the thickest silica shells, faster *Z*–*E* conversion is detected after allowing azobenzene molecules to diffuse inside the silica layer overnight (Fig. 8-B and S8†). This indicates a non-stationary diffusion regime for AB molecules in silica shells thicker than 2.7 ± 0.6 nm immediately after NP addition. Insets of Fig. 8 show the log data representation for the exponential growth phase of the kinetic traces. Parallel curves point to the stationary state diffusion regime for AB in the silica layer. Distinctively, for 2.7 ± 0.6 nm silica shell thickness, parallelism of both plots is observed, while the thicker the silica layer, the higher is the ratio of slopes between the incubated and the as-prepared samples. This ratio is 2 for 4 ± 1 nm thickness and 3 for 7 ± 1 nm, 13 ± 1 nm, and 15 ± 2 nm silica layers.

Discussion

The kinetics and mechanism of the catalyzed thermal back isomerization of azobenzenes in AuNP suspensions are analyzed by studying the dependence of k_{obs} as a function of the relative AB–AuNP concentration (see Fig. S7† and 5).

To interpret the physicochemical meaning of the observed first order rate constant, we propose a compartmentalized reaction scenery (see Scheme 1) where the *Z* and *E* isomers are distributed in two phases, the dispersed phase (formed by the sum of the volume of influence of all the AuNPs) and the continuous (solvent) phase. Assuming rapid equilibration

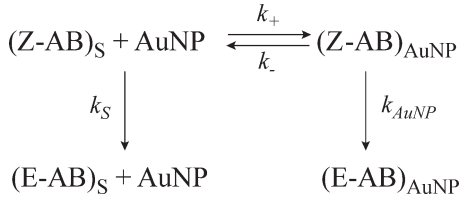

Scheme 1 Mechanism for the microheterogeneous dark *Z–E* isomerization catalyzed by AuNPs.

for the reactant exchange steps between compartments compared to the reactive steps (*i.e.* $k_+[Z\text{-AB}]_S$, $k_- \gg k_S$, and k_{AuNP}), and neglecting reactant exchange by direct AuNP interactions, the first order reaction rate constant can be expressed as a weighted average of the first order isomerization rate constants in solution, k_S, and in the vicinity of AuNPs, k_{AuNP} (uncatalyzed and catalyzed reaction pathways, respectively). The weighting factors are the mole fractions of *Z*-AB molecules associated with each phase. Further, expressing the concentration of the *Z* isomer in the disperse phase as a function of the average number of *Z* molecules associated with each single AuNP, $\langle n \rangle$, the following expression for k_{obs} can be obtained (see S6†),

$$k_{obs} = k_S + \frac{\langle n \rangle [AuNP]}{[Z\text{-AB}]_T} \cdot (k_{AuNP} - k_S) \quad (1)$$

where $[Z\text{-AB}]_T$ is the total concentration of the *Z*-AB isomer obtained immediately after flash photolysis. This parameter is evaluated from the difference absorption spectrum.

For all the studied azobenzenes and for all the combinations of [AuNP]/[AB] tested it holds that $k_{obs} \gg k_S$, accordingly $k_{AuNP} \gg k_S$, and therefore, eqn (1) can be simplified to eqn (2),

$$k_{obs} = \frac{\langle n \rangle [AuNP]}{[Z\text{-AB}]_T} \cdot k_{AuNP} \quad (2)$$

Fig. 5 displays the inverse of k_{obs} as a function of $[Z\text{-AB}]_T/[AuNP]$ for different azobenzene–AuNP systems. As expected, the increase of k_{obs} as a function of $[AuNP]/[Z\text{-AB}]_T$ is related to the higher proportion of *Z*-AB molecules associated with the disperse phase. The linear relationship observed in Fig. 5 suggests that $\langle n \rangle$ is a constant value in the concentration range tested.

The experiments with PVP blocking the {100} facets give the hint of the predominant surface character of the catalysis and point to these planes as the more catalytically active ones. The experiments performed with AuNPs@SiO_2 suspensions allowed further elucidation of the spatial catalytic extension of the AuNPs. Particularly, it was possible to determine whether the isomerization catalysis was active at nanometer distance from the AuNP surface or if it only takes place upon direct contact with the metallic surface. The distinct catalytic behavior for even the thinner silica shell AuNPs@SiO_2 with respect to the bare NPs as well as the competitive experiments with PVP enlightens the surface catalytic nature of the AuNPs on the *Z–E* isomerization in azobenzenes. On the other hand, the constant average number of *Z* molecules associated with each single AuNP evidenced in the kinetic experiment can be considered as the maximum number of available adsorption sites in the surface of each AuNP, n_{max}. This latter parameter can be estimated using different assumptions. In this work, it was approximated as 10^3 binding sites for a 15 nm diameter AuNP and considered independent of the derived structure of the azobenzene (see S7† for detailed calculation).

The acceleration of the reaction rate constant measured on Au {100} facets is in line with the reported reduction of the activation energy by a factor of four for the thermal *Z–E* isomerization of adsorbed tetra-*tert*-butyl-azobenzene on Au {111} compared to the free molecule in the liquid phase.[22] In another work, the authors find a change in the lifetime of 3-(4-(4-hexyl-phenylazo)-phenoxy)-propane-1-thiol from more than 35 h in dichloromethane solution to *ca.* 60 s in a self-assembled mixed monolayer with *n*-butanethiol on Au {111}.[23]

Table 1 reports the values of k_{AuNP} calculated from the best linear fit of the experimental data of Fig. 5. The enhancement factor in k_{AuNP} for AB and MO-AB in aqueous suspensions of AuNPs is in the order of 10^5. On the other hand, DM-AB, DC-AB and DEO-AB show a 10^3-fold acceleration in suspensions of ACN : water (5 : 1). Further, NO_2 substituted azobenzenes only show a 10^2 or 10^1 AuNP catalytic factor in the same solvent mixture.

The acceleration of the reaction rate induced by AuNPs is related to the weakening of the azo double bond character on the surface of the gold nanoparticle.[4] Azobenzenes carrying an electronegative group present intrinsically a weaker –N–N– double bond character and therefore the expected AuNP catalytic effect should be poorer. However, if we only consider the electronegativity factor of the azobenzene substituents, we cannot explain the acceleration observed for the MO-AB *Z–E* thermal isomerization relative to the symmetrically substituted azobenzenes such as DM-AB or DC-AB. To give an explanation for this fact, we should take into account that ACN is reversibly adsorbed on the gold surface with a binding energy of 46 kJ mol^{-1} onto the Au(100) facets,[24] thus competing with the azobenzene molecules for the adsorption sites (E_{ad} ~ 160 kJ mol^{-1} for Au(111)).[25] Therefore, decrease in the global isomerization reaction rate constant for systems measured in ACN : water (5 : 1) with respect to the ones measured in water can be attributed to a decrease in the value of

Table 1 Parameters of the best linear fit of the inverse of eqn (2) for the experimental data of Fig. 5

Azobenzene	$n_{max}\ k_{NP}$ (s^{-1})	k_{NP}[a] (s^{-1})	k_S (s^{-1})	k_{NP}/k_S
AB	1×10^3	1×10^0	1×10^{-6}	1×10^6
DM-AB	4×10^1	4×10^{-2}	7×10^{-6}	6×10^3
DC-AB	2×10^1	2×10^{-2}	6×10^{-6}	4×10^3
DEO-AB	6×10^1	6×10^{-2}	3×10^{-5}	2×10^3
MO-AB	3×10^3	3×10^0	6×10^{-6}	5×10^5
NO_2-AB	3×10^1	3×10^{-2}	1×10^{-4}	2×10^2
NO_2-MOAB	5×10^1	5×10^{-2}	1×10^{-3}	4×10^1

[a] Obtained considering in all cases $n_{max} = 10^3$ (see S7†).

Table 2 Diffusion rate constant, k_{diff}, and diffusion coefficient, $D_{AB\text{-}SiO_2}$, for AB molecules in silica as a function of silica shell thickness, h_{SiO_2}. k_{diff} was determined with the best monoexponential fit of the data of Fig. 7 and S8† (grey circles). The $D_{AB\text{-}SiO_2}$ was calculated using eqn (3)

h_{SiO_2} (nm)	k_{diff} (10^{-3} s^{-1})	$D_{AB\text{-}SiO_2}$ (10^{-11} cm^2 s^{-1})
2.7 ± 0.6 nm	0.68	1.1 ± 0.5
4 ± 1 nm	0.82	1.6 ± 0.7
7 ± 1 nm	1.6	5 ± 2
13 ± 1 nm	1.8	11 ± 4
15 ± 2 nm	1.9	8 ± 3

n_{max}. Further, the NO_2 groups can also be reversibly adsorbed on the gold surface (E_{ad} ~ 58.6 kJ mol^{-1} for Au(111))[26] and therefore compete with the azo moiety for the surface binding sites, without the same effect in the reactive rate.

Finally, we can use the kinetic curves in AuNPs@SiO_2 to estimate the diffusion coefficient of AB in silica, $D_{AB\text{-}SiO_2}$, by solving Fick's equation for steady state diffusion in a spherical geometry (see S8†). Eqn (3) holds for the $D_{AB\text{-}SiO_2}$ as a function of the diffusion kinetic rate constant, k_{diff}, the AuNPs radius, r_{NP}, the thickness of the silica shell, h_{SiO_2}, and [AuNPs].

$$D_{AB\text{-}SiO_2} = \frac{k_{diff}}{4\pi \cdot [AuNP] \cdot N_A} \cdot \frac{h_{SiO_2}}{r_{NP}(r_{NP} + h_{SiO_2})} \quad (3)$$

Table 2 summarizes k_{diff} and $D_{AB\text{-}SiO_2}$ for the different silica shell thicknesses. The small diffusion coefficient for AB in silica (~10^{-10}–10^{-11} cm^2 s^{-1}) in comparison to free diffusion of AB in water (~10^{-6} cm^2 s^{-1})[27] is related to the tortuous pathway for diffusing molecules inside the disordered and microporous silica shell (estimated porous size of ~15 Å).[28] Further, the hydrophilic silica pores (active hydroxyl groups) may promote the adsorption of molecules in the silica pores (chemical traps) precluding the arrival of *Z*-AB molecules to the gold surface. As regards the higher $D_{AB\text{-}SiO_2}$ values for thicker silica shells, this can be understood as a more compact silica matrix for the proximal layers compared to the more expanded outer part.

Conclusions

Z–E thermal isomerization reaction of 4 or 4-4′ substituted azobenzenes is highly accelerated in sub-nanomolar 15 ± 1 nm diameter AuNP suspensions. Microheterogeneous kinetic analysis was found useful to describe the combined process of the thermal *Z* isomer decay in the continuous solution phase and under the catalytic influence of the dispersed AuNPs. With this approach it was possible to determine the first order isomerization rate constants in the vicinity of AuNPs. The magnitude of the acceleration is determined not only by the nature of the substituents but also by the solvent and surfactants present in the reaction medium. The maximum acceleration factor detected, of 10^6 times, was for AB in aqueous solution and in the absence of external surfactants. The competitive adsorption of acetonitrile, polyvinylpyrrolidone (PVP) and NO_2 groups in the azo moiety binding sites of the gold surface masks the AuNP catalytic effect. Selective blocking experiments with PVP suggested that the {100} crystalline facets are particularly active for the catalysis. Experiments performed with core–shell AuNPs with different silica spacers around the gold surface reveal the exclusive surface nature of the AuNP mediated catalysis. Further, it was possible to determine the diffusion coefficient of AB in silica layers as $D_{AB\text{-}SiO_2}$ ~ 10^{-10}–10^{-11} cm^2 s^{-1}.

Experimental

Chemicals

All reagents given as follows were used as received unless specified otherwise: $HAuCl_4 \cdot 3H_2O$ (≥99.9%, Aldrich), trisodium citrate dihydrate (≥99%, Aldrich), 2-hydroxy-4′-(2-hydroxyethoxy)-2-methylpropiophenone (Irgacure 2959) (98%, Aldrich), tetraethyl orthosilicate (≥98.0%, Fluka) (TEOS), (3-aminopropyl)triethoxysilane (≥98%, Sigma Aldrich), polyvinylpyrrolidone (PVP10) (average molecular weight, 10 000 g mol^{-1}, Sigma Aldrich), acetonitrile (HPLC grade, Sintorgan), azobenzene (98%, Sigma Aldrich) (AB), 4-methoxyazobenzene (≥99.0%, Aldrich) (MO-AB), 4-nitroazobenzene (90%, Aldrich) (NO_2-AB), 4,4′-dimethylazobenzene (Aldrich^{CPR}) (DM-AB), 4,4′-dichloroazobenzene (Aldrich^{CPR}) (DC-AB), 4,4′-diethoxyazobenzene (97%, ALFA AESAR) (DEO-AB), 4-nitro-4′-methoxyazobenzene (NO_2-MOAB), 4-nitro-4′-dimethylaminoazobenzene (≥98.0%, TCI) (NO_2-DAB), 4-(4′-nitrophenylazo)phenol (≥97.0%, TCI) (NO_2-HAB), and 4-[4-(dimethylamino)phenylazo]benzoic acid *N*-succinimidyl ester (Sigma Aldrich) (DABCYL). All of the following reagents were of analytical grade: hydrochloric acid, ammonia, ethanol, and sodium hydroxide.

Nanoparticle synthesis

Au nanoparticles with an average radius of 15 ± 1 nm (see Fig. 1) were prepared following the Turkevich protocol.[29] 'Semi-naked' gold nanoparticles were photochemically synthesized as described elsewhere[30] obtaining nanoparticles with a mean radius of 10 ± 2 nm (see Fig. S1†). Au–SiO_2 core–shell nanoparticles (AuNP@SiO_2) of 2.7 ± 0.6, 4 ± 1, 7 ± 1, 13 ± 1, and 15 ± 2 nm silica shell thicknesses (see Fig. 1-B to F) were synthesized following the van Blaaderen procedure.[31] Briefly, PVP10 was used as a coupling agent to transfer the colloids from water to a 4.2% v/v ammonia–ethanol medium. Silica deposition over the gold core was performed by quickly adding TEOS under vigorous stirring. The solution was kept under stirring at room temperature for 12 h. The silica-coated nanoparticles were purified by 3 cycles of redispersion in ethanol and centrifugation at 12 000 RCF. The final concentration of the nanoparticle solution was determined by gold quantification of the nanoparticle suspension with a graphite furnace atomic absorption spectrometer. Silica nanoparticles (mean radius = 71 ± 8 nm, see Fig. S2†) employed as control samples were prepared following a standard Stöber protocol.[32]

Spectroscopy

UV-VIS spectra were measured on a Hewlett Packard 8452A, on a Shimadzu UV3101PC (Shimadzu Corporation, Kyoto, Japan), or on a Cary 50 UV-Vis (Agilent Technologies, Santa Clara, USA). Laser flash photolysis experiments were carried out using a Surelite-II OPO Plus (a pump with a Nd-YAG at 355 nm) (Continuum, Santa Clara, USA) as the excitation source. Data were recorded with a LFP 111 laser-flash photolysis system (Luzchem Inc., Ottawa, Canada).

System characterization

Nanoparticle mean radius and silica shell thickness were measured by either transmission electron microscopy (TEM) using a Philips EM 301 apparatus or scanning electron microscopy (SEM) using a JEOL JSM-7500F.

Sample preparation

Typical experiments were performed in 1 cm × 1 cm quartz cuvettes combining 50 to 500 μL of AuNPs or AuNP@SiO_2 with water or ethanol or mixtures of acetonitrile–water until a final volume of 3 mL was reached. Kinetic experiments were performed after gradual addition of 5 to 45 μL of 5 mM or 1 mM ACN solutions of the corresponding AB to the previous mentioned NP suspension. All azobenzenes/AuNP suspensions except for AB and MO-AB were prepared in 5 : 1 ACN : water mixtures. *E–Z* photochemical conversion was performed with either a commercial photographic xenon flash lamp or with the corresponding excitation wavelength of the OPO laser. For the pH dependence experiments solutions of HCl or NaOH were also used.

Acknowledgements

PFA is a research staff and SS is a research fellow from CONICET. The work was performed under support from CONICET (PIP 11220100100397) and UBA (grant number: 20020100100234). SS acknowledges ELAP (Emerging Leaders in the Americas Program) for the DFAIT fellowship that supported her visit to Canada. We thank Prof. Juan C. Scaiano (University of Ottawa) for helpful suggestions and for providing the facility used to perform the laser flash photolysis experiments and to synthesize the 'semi-naked' gold nanoparticles.

Notes and references

1 R. Klajn, J. F. Stoddart and B. A. Grzybowski, *Chem. Soc. Rev.*, 2010, **2039**, 2203–2237.
2 Y. B. Zheng, Y.-W. Yang, L. Jensen, L. Fang, B. K. Juluri, A. H. Flood, P. S. Weiss, J. F. Stoddart and T. J. Huang, *Nano Lett.*, 2009, **9**, 819–825.
3 S. J. van der Molen, J. Liao, T. Kudernac, J. S. Agustsson, L. Bernard, M. Calame, B. J. van Wees, B. L. Feringa and C. Schönenberger, *Nano Lett.*, 2008, **9**, 76–80.
4 J. H. Yoon and S. Yoon, *Phys. Chem. Chem. Phys.*, 2011, **13**, 12900–12905.
5 R. Klajn, K. J. M. Bishop and B. A. Grzybowski, *Proc. Natl. Acad. Sci. U. S. A.*, 2007, **104**, 10305–10309.
6 D. S. Sidhaye, S. Kashyap, M. Sastry, S. Hotha and B. L. V. Prasad, *Langmuir*, 2005, **21**, 7979–7984.
7 E. Dulkeith, A. C. Morteani, T. Niedereichholz, T. A. Klar, J. Feldmann, S. A. Levi, F. C. J. M. van Veggel, D. N. Reinhoudt, M. Möller and D. I. Gittins, *Phys. Rev. Lett.*, 2002, **89**, 203002.
8 J. Zhang, J. K. Whitesell and M. A. Fox, *Chem. Mater.*, 2001, **13**, 2323–2331.
9 K. Shin and E. J. Shin, *Bull. Korean Chem. Soc.*, 2008, **29**, 1259–1262.
10 A. Manna, P.-L. Chen, H. Akiyama, T.-X. Wei, K. Tamada and W. Knoll, *Chem. Mater.*, 2003, **15**, 20–28.
11 G. L. Hallett-Tapley, C. D'Alfonso, N. L. Pacioni, C. D. McTiernan, M. González-Béjar, O. Lanzalunga, E. I. Alarcon and J. C. Scaiano, *Chem. Commun.*, 2013, **49**, 10073–10075.
12 N. Nishimura, T. Sueyoshi, H. Yamanaka, E. Imai, S. Yamamoto and S. Hasegawa, *Bull. Chem. Soc. Jpn.*, 1976, **49**, 1381–1387.
13 P. P. Birnbaum, J. H. Linford and D. W. G. Style, *Trans. Faraday Soc.*, 1953, **49**, 735–744.
14 G. S. Hartley, *J. Chem. Soc.*, 1938, 633–642.
15 N. J. Dunn, W. H. Humphries, A. R. Offenbacher, T. L. King and J. A. Gray, *J. Phys. Chem. A*, 2009, **113**, 13144–13151.
16 A. M. Sanchez and R. H. Rossi, *J. Org. Chem.*, 1995, **60**, 2974–2976.
17 S. Ciccone and J. Halpern, *Can. J. Chem.*, 1959, **37**, 1903–1910.
18 H. S. Taylor, *Proc. R. Soc. London, Ser. A*, 1925, **108**, 105–111.
19 S. M. Oxford, J. D. Henao, J. H. Yang, M. C. Kung and H. H. Kung, *Appl. Catal., A*, 2008, **339**, 180–186.
20 M. M. Nigra, I. Arslan and A. Katz, *J. Catal.*, 2012, **295**, 115–121.
21 Y. Sun, B. Mayers, T. Herricks and Y. Xia, *Nano Lett.*, 2003, **3**, 955–960.
22 S. Hagen, P. Kate, M. V. Peters, S. Hecht, M. Wolf and P. Tegeder, *Appl. Phys. A: Mater. Sci. Process.*, 2008, **93**, 253–260.
23 U. Jung, O. Filinova, S. Kuhn, D. Zargarani, C. Bornholdt, R. Herges and O. Magnussen, *Langmuir*, 2010, **26**, 13913–13923.
24 T. Solomun, K. Christmann and H. Baumgaertel, *J. Phys. Chem.*, 1989, **93**, 7199–7208.
25 E. R. McNellis, J. Meyer and K. Reuter, *Phys. Rev. B: Condens. Matter Mater. Phys.*, 2009, **80**, 205414.
26 M. E. Bartram and B. E. Koel, *Surf. Sci.*, 1989, **213**, 137–156.
27 W. Dozier, J. Drake and J. Klafter, *Phys. Rev. Lett.*, 1986, **56**, 197–200.
28 A. van Blaaderen and A. Vrij, *J. Colloid Interface Sci.*, 1993, **156**, 1–18.
29 J. Turkevich, P. C. Stevenson and J. Hillier, *Discuss. Faraday Soc.*, 1951, **11**, 55–75.
30 K. L. McGilvray, J. Granger, M. Correia, J. T. Banks and J. C. Scaiano, *Phys. Chem. Chem. Phys.*, 2011, **13**, 11914–11918.
31 C. Graf, D. L. J. Vossen, A. Imhof and A. van Blaaderen, *Langmuir*, 2003, **19**, 6693–6700.
32 W. Stöber, A. Fink and E. Bohn, *J. Colloid Interface Sci.*, 1968, **26**, 62–69.